

Putative quantum critical point in locally noncentrosymmetric CeCoGe₂ crystals

F. Garmroudi,¹ C. S. T. Kengle,¹ M. H. Schenck,^{1,2} J. D. Thompson,¹ E. D. Bauer,¹ S. M. Thomas,¹ and P. F. S. Rosa¹

¹*Materials Physics Applications–Quantum, Los Alamos National Laboratory, Los Alamos, New Mexico 87545, USA*

²*Department of Physics, Colorado State University, Fort Collins, Colorado 80523, USA*

Locally noncentrosymmetric heavy-fermion compounds may produce long-sought correlated quantum phases, such as spin-triplet superconductivity with non-Abelian quasiparticles, but identifying the right candidate systems is challenging. Here, using the In flux method, we synthesize CeCoGe₂ single crystals, belonging to the highly tunable pseudotetragonal (*Cmcm*) CeTX₂ family, which allows for substitutions at both the transition metal *T* and at the *X* sites. We identify a heavy-fermion ground state with a Sommerfeld coefficient $\gamma \approx 120 \text{ mJ mol}^{-1} \text{ K}^{-2}$ and a non-Fermi-liquid exponent of the electrical resistivity, which may indicate its proximity to the putative quantum critical point. However, no signs of superconductivity or magnetic order are detected down to 20 mK. Our analysis of electrical transport and structural properties indicates that coherent charge transport and the emergence of superconductivity observed under hydrostatic pressure in related compounds (CePtSi₂ and CeRhGe₂) are suppressed in CeCoGe₂ by strong random potential scattering due to intrinsic Co vacancies (approximately 4% even in the highest-quality crystals). By tuning the growth stoichiometry and temperature profile, we demonstrate that the defect concentration can be controlled and has a pronounced effect on the residual resistivity. We hypothesize that superconductivity may be found in higher-quality CeCoGe₂ crystals grown by different techniques.

I. INTRODUCTION

The study of *4f* and *5f* electron-based heavy-fermion compounds has long been a fertile ground for exploring the rich interplay between strong electronic correlations, magnetism, and the exotic quantum phases emerging therefrom [1–6]. One of the most intriguing phenomena emerging from this interplay is spin-triplet superconductivity – an unconventional and exceptionally rare superconducting state in which Cooper pairs form odd-parity orbital wavefunctions, in contrast to the spin-singlet, even-parity pairing in conventional superconductors [7–11]. Beyond its fundamental interest, such a superconducting state can exhibit nontrivial topological properties, giving rise to exotic quasiparticles such as Majorana zero modes, which are considered promising platforms for realizing topologically protected, fault-tolerant quantum computation [12–14]. In particular, the realization of a chiral, multicomponent $p_x + ip_y$ pairing state has been a long-standing goal [15–17]. In two dimensions, such a pairing symmetry would be fully gapped, allowing the Majorana zero modes to be protected and energetically separated from other low-energy excitations.

Key structural ingredients to realize such an exotic superconductor in a bulk heavy-fermion material appear to be (i) local inversion symmetry breaking in a globally centrosymmetric crystal structure; more specifically, there should exist two or more *f*-electron ions per unit cell related in pairs by inversion [18, 19] and (ii) a two-dimensional, layered crystal structure, where superconductivity in the layers is sufficiently immune to interlayer coupling. Among all known spin-triplet superconductor candidates, the majority are *f*-electron materials, with only a handful of U-based compounds (UBe₁₃ [20, 21], UPt₃ [22], U(Co,Rh)Ge [23, 24], U₂PtC₂ [25] and UTe₂ [11, 26]) and only a single Ce-based system (CeRh₂As₂ [27]) displaying signatures of spin-triplet superconduc-

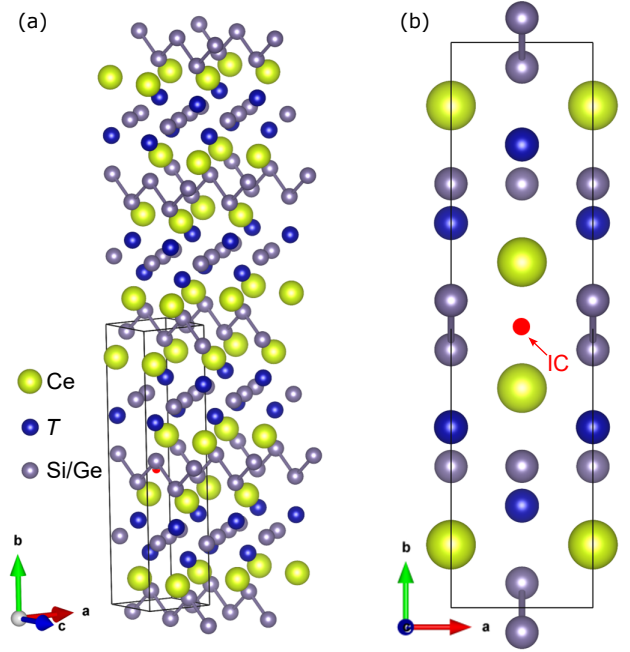


FIG. 1. (a) Pseudotetragonal crystal structure ($a \approx c \ll b$) of CeTX₂ (*T* being a transition metal and *X* = Si, Ge) with the locally noncentrosymmetric CeNiSi₂ structure (*Cmcm*). (b) Ce atoms are positioned around an inversion center (IC) located in the middle of the unit cell.

tivity at ambient pressure. Additionally, a few other systems have been identified under pressure [28–32]. However, none of these materials has been shown to realize the sought-after $p_x + ip_y$ pairing state. It is thus crucial to identify and systematically screen other candidates.

Here, we investigate CeCoGe₂ belonging to the CeTX₂ family (*T* being a transition metal and *X* = Si, Ge), which crystallize in the pseudotetragonal, orthorhombic

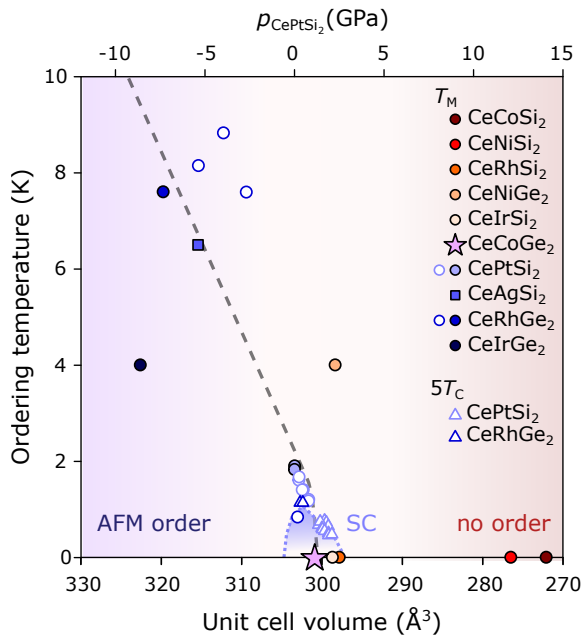


FIG. 2. Phase diagram and putative quantum critical point in locally noncentrosymmetric $CeTX_2$. Chemical (filled symbols) and hydrostatic (open symbols) pressure tune the magnetic ground state from antiferromagnetic order for a unit-cell volume $V \gtrsim 300 \text{ \AA}^3$ to paramagnetic states for $V \lesssim 300 \text{ \AA}^3$. A superconducting dome emerges for $CePtSi_2$ and $CeRhGe_2$ under hydrostatic pressure, centered around $V_c \approx 300 \text{ \AA}^3$, which corresponds to the unit-cell volume of $CeCoGe_2$.

bic ($Cmcm$) $CeNiSi_2$ structure [Fig. 1(a)], which has an inversion center in the center of the unit cell with Ce atoms occupying sites that lack local inversion symmetry [see Fig. 1(b)] [33, 34]. The hybridization between the localized Ce $4f$ states and the conduction electrons in these systems, is highly sensitive to the unit-cell volume (V), giving rise to antiferromagnetically-ordered states for $V \gtrsim 300 \text{ \AA}^3$ [34–38] and paramagnetic ground states if the unit-cell volume is less than $\approx 300 \text{ \AA}^3$ (see Fig. 2) [39–42]. In addition, the period of the transition metal strongly affects the c - f hybridization, with $3d$ transition metals favoring more localized, magnetic behavior, whereas the $5d$ elements tend to promote delocalization (compare for instance $CeNiGe_2$ and $CeIrGe_2$ in Fig. 2). It has been shown that both $CePtSi_2$ and $CeRhGe_2$ become superconducting when their unit-cell volume is tuned via hydrostatic pressure to a putative quantum critical point (QCP) [37, 43]. Using pressure-dependent x-ray diffraction data for $CePtSi_2$ from Ref. [44], we convert hydrostatic pressure to unit-cell volume and find that the critical pressures, $p_c \approx 1.2 \text{ GPa}$ for $CePtSi_2$ [43] and $p_c \approx 7 \text{ GPa}$ for $CeRhGe_2$ [37], correspond to a common critical volume of $V_c \approx 300 - 301 \text{ \AA}^3$. Nakano *et al.* first demonstrated pressure-induced superconductivity in polycrystalline $CePtSi_2$ [43], and Hirose *et al.* subsequently extended their study on single crystals [37]. We note that, although not explicitly discussed in Ref. [37],

their findings suggest strongly enhanced upper critical fields that exceed the Pauli limiting field by nearly an order of magnitude – a hallmark of spin-triplet superconductivity. Together with the essential symmetry ingredients in the crystal structure, these observations make a case for $CePtSi_2$ and $CeRhGe_2$ as candidate spin-triplet superconductors under pressure.

Plotting the magnetic and superconducting transition temperatures of various $CeTX_2$ systems versus their unit-cell volume (Fig. 2) further suggests that among all these compounds, $CeCoGe_2$ is positioned closest to the putative QCP and the associated superconducting dome. However, to date, no experimental studies below 2 K have been reported on $CeCoGe_2$, and superconductivity in $CePtSi_2$ and $CeRhGe_2$ emerges only at much lower temperatures ($T_C \approx 0.14 \text{ K}$) [37]. Moreover, previous investigations of $CeCoGe_2$ have been limited to arc-melted polycrystalline samples of relatively poor quality [45]. These considerations motivated the present study in which we investigate the low-temperature physical properties of $CeCoGe_2$ single crystals and search for signatures of superconductivity.

This paper is organized as follows. First, we present and discuss the magnetic (section III A), thermodynamic (III B), and electrical transport properties (III C) of $CeCoGe_2$ single crystals grown by the In-flux method and compare our results to those obtained previously on polycrystalline samples. Then, in section III D, we address the role of persistent intrinsic Co vacancies and describe our attempts to suppress them by controlling the starting stoichiometry and the temperature profile during crystal growth. We ascribe the absence of superconductivity in $CeCoGe_2$ to strong disorder scattering of charge carriers induced by these vacancies.

II. EXPERIMENTAL METHODS

A. Crystal growth

$CeCoGe_2$ single crystals were grown from In flux. Polycrystalline precursor ingots were first prepared by arc melting stoichiometric amounts of Ce (99.95%), Co (99.95%) and Ge (99.9999%) under an inert Ar atmosphere. The resulting ingots were crushed and hand-ground into a coarse powder, which was subsequently mixed with In in a molar ratio of 1:30. The mixtures were loaded into alumina crucibles, sealed in evacuated quartz tubes, and heated to $1150 \text{ }^\circ\text{C}$ at a rate of $100 \text{ }^\circ\text{C/h}$. After homogenization at this temperature for 48 h, the samples were slowly cooled to $700 \text{ }^\circ\text{C}$ at a rate of $2 \text{ }^\circ\text{C/h}$. The excess In flux was removed by centrifugation, and residual flux was eliminated by etching the crystals in diluted hydrochloric acid. The obtained crystals were plate-like, with thicknesses of up to a few hundred micrometers and lateral dimensions of up to a few square millimeters. The crystallographic orientation of the samples was determined using a Photonic Sci-

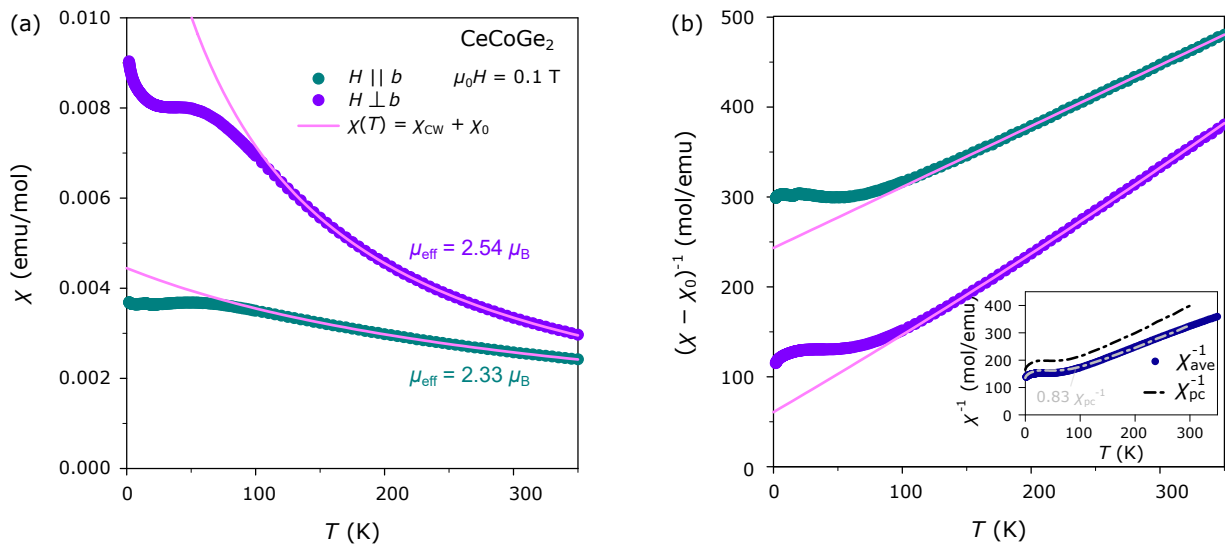


FIG. 3. Temperature-dependent (a) magnetic susceptibility and (b) inverse susceptibility of a plate-like CeCoGe₂ single crystal as grown from indium flux. There exists magnetic anisotropy with χ being about two times larger perpendicular to the crystallographic b axis compared to measurements with an applied field parallel to b . Modified Curie-Weiss fits of $\chi(T)$ at temperatures above ≈ 150 K yield effective magnetic moments of $2.54 \mu_B$ and $2.33 \mu_B$ for $H \perp b$ and $H \parallel b$, respectively. Inset in (b) shows the single crystal average $\chi_{\text{ave}} = \frac{2}{3}\chi_{\perp b} + \frac{1}{3}\chi_{\parallel b}$ compared to data for polycrystalline arc-melted samples by Mun *et al.* [45]. Scaling the polycrystalline data by a factor 0.83, which corresponds to the phase purity of polycrystalline samples synthesized in the course of this work following the same recipe as in Ref. [45], yields near-perfect agreement with χ_{ave} .

ence Laue diffractometer, and the composition and microstructure were investigated in a scanning electron microscope equipped with a back-scattered electron detector and energy dispersive x-ray spectroscopy. The latter revealed homogeneous microstructures with uniform elemental distributions and no detectable impurity phases or residual flux.

B. Characterization

Single-crystal x-ray diffraction experiments were conducted at room temperature using a Bruker D8 Venture diffractometer equipped with an Incotec $I\mu\text{S}$ microfocus source using Mo K- α radiation ($\lambda = 0.71073 \text{ \AA}$). Data were collected using a PHOTON II CPAD detector and processed using Bruker SAINT software. The initial crystallographic model was obtained via intrinsic phasing methods in SHELXT. The refined structures were obtained via least-squares refinements using SHELXL2018. For as grown CeCoGe₂ crystals, our refinements yield a unit cell volume of $300.12(11) \text{ \AA}^3$. After annealing at 600°C for one week, we see a volume contraction of the unit cell down to $297\text{--}298 \text{ \AA}^3$ for the annealed crystals. Specific heat and magnetic measurements were performed for the as-grown crystals, while electrical resistivity was measured for both as-grown and annealed crystals, revealing comparable residual resistivities and overall behavior but slightly modified low-temperature exponents as discussed in section III C.

Magnetic susceptibility (χ) and magnetization (M)

measurements were carried out in a Quantum Design (MPMS3) magnetometer using the VSM mode. Susceptibility was measured in a field of 1 kOe applied parallel and perpendicular to a single crystal's b -axis. Magnetization measurements at 1.8 K were linear in field to 65 kOe for both crystal orientations and showed the same anisotropy as χ (see Fig. 7 in the Appendix).

Heat-capacity measurements were performed using the two-tau thermal relaxation method in a Quantum Design Physical Property Measurement System (PPMS). For measurements below 1.8 K and down to 0.37 K, a ^3He refrigerator insert was employed. The electrical resistivity from 1.8 to 300 K and up to 5 T was also measured in a PPMS making use of a standard four-probe configuration with platinum wires spot-welded to the CeCoGe₂ single crystals. Resistivity measurements down to 0.02 K were performed in a Proteox dilution refrigerator.

III. RESULTS AND DISCUSSION

A. Magnetic susceptibility

Figure 3 shows the magnetic susceptibility [Fig. 3(a)] and inverse susceptibility [Fig. 3(b)] of an as-grown, plate-like CeCoGe₂ single crystal, measured with magnetic fields ($\mu_0 H = 0.1 \text{ T}$) applied perpendicular ($H \perp b$) and parallel ($H \parallel b$) to the crystallographic b direction. It can be seen that there exists sizeable magnetic anisotropy, with $\chi_{\perp b}$ being approximately two times larger than $\chi_{\parallel b}$, opposite to CeNiGe₂, CeRhGe₂ and

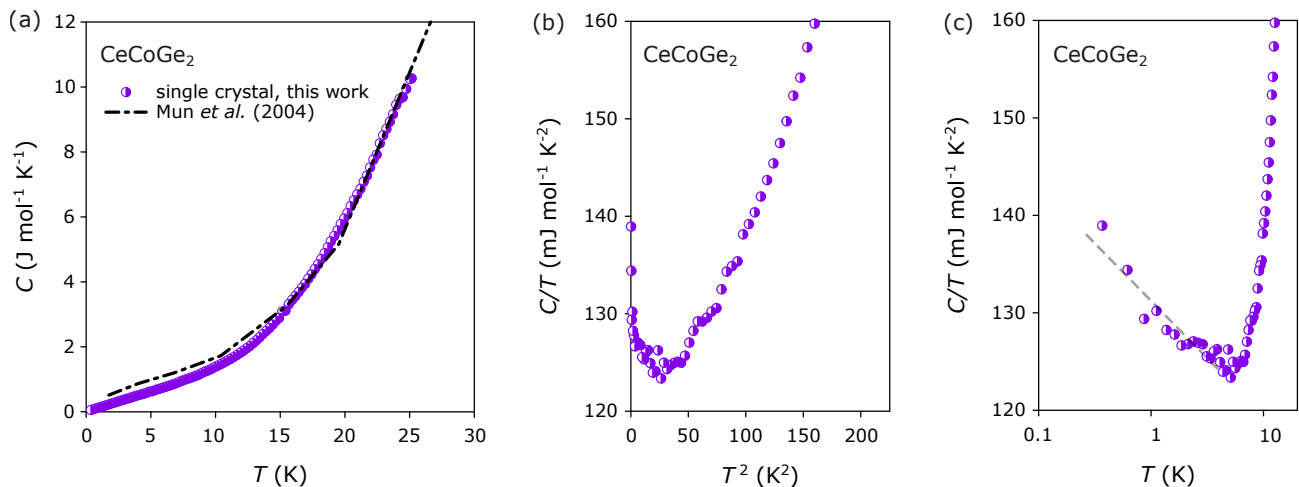


FIG. 4. Low-temperature specific heat of CeCoGe₂. (a) Comparison of as-grown CeCoGe₂ single crystals from this work and arc-melted polycrystalline samples from Ref. [45]. (b) The low-temperature slope of the specific heat C/T , measured down to 0.37 K, reveals a heavy-fermion ground state with a Sommerfeld coefficient of around 120 mJ mol⁻¹ K⁻² and an additional upturn of C/T at the lowest temperatures, which, as shown in (c), roughly follows a logarithmic behavior.

CePtSi₂, where $\chi_{\perp b} \ll \chi_{\parallel b}$ [36, 37]. We fit the high-temperature data using a modified Curie-Weiss law,

$$\chi(T) = \chi_{\text{CW}} + \chi_0 = C/(T - \theta) + \chi_0. \quad (1)$$

Here, θ represents the paramagnetic Curie-Weiss temperature, $C = (N_A \mu_{\text{eff}}^2)/(3k_B)$ and $\chi_0 = \chi_{\text{P}} + \chi_{\text{dia}}$ is a constant term including Pauli-paramagnetic and diamagnetic contributions. From our fits, $\chi_0 \approx 3 - 4 \times 10^{-4}$ emu/mol for both field directions. Moreover, we determine effective moments of around $\mu_{\text{eff}} \approx 2.54 \mu_B$ for $H \perp b$, in excellent agreement to the value for the free Ce³⁺ ion, and $\mu_{\text{eff}} \approx 2.33 \mu_B$ for $H \parallel b$, slightly smaller than the free-ion value ($2.54 \mu_B/\text{Ce}$) with large negative Curie-Weiss temperatures, $\theta \approx -74$ K and -359 K for $H \perp b$ and $H \parallel b$, respectively. Since $\theta_{H \parallel b}$ exceeds the temperature range over which the fit was performed, there is likely a sizeable uncertainty in the fitted value of μ_{eff} for $H \parallel b$.

Below 100 K, $\chi(T)$ develops a shallow bump, which may be attributed to crystal electric field (CEF) excitations, followed by an additional upturn at the lowest temperatures, likely due to magnetic impurities. Because a similar Curie tail at low temperatures has been observed in LaCoGe₂ [45], it is possible that these features stem from small amounts of Co-based impurity phases or magnetic defects related to the Co sublattice.

We also calculated the average susceptibility $\chi_{\text{ave}} = \frac{2}{3}\chi_{\perp b} + \frac{1}{3}\chi_{\parallel b}$ obtained by averaging the single-crystal data and compared it to the polycrystalline data by Mun *et al.* [45] in the inset of Fig. 3(b). Since $a = 4.25 \text{ \AA} \approx c = 4.20 \text{ \AA} \ll b = 16.74 \text{ \AA}$, no significant anisotropy is expected in the ac plane – the lack of which was also confirmed for CeNiGe₂, CeRhGe₂ and CePtSi₂. We find that χ_{ave} is in good agreement with χ_{pc} from Ref. [45], especially after scaling by a constant factor of 0.83 [grey line in Fig. 3(b)], which roughly corresponds to the phase

purity (80 – 90 %) of polycrystalline samples synthesized and investigated in the course of this work following the exact same recipe as in Ref. [45].

B. Specific heat

In Fig. 4, we show the low-temperature specific heat $C(T)$ of CeCoGe₂. Above 2 K, our data are in excellent agreement with previously reported results on arc-melted polycrystalline samples by Mun *et al.* [45] [see Fig. 4(a)], exhibiting a pronounced linear term below 10 K that corresponds to a Sommerfeld coefficient of $\gamma \approx 120$ mJ mol⁻¹ K⁻², consistent with a heavy-fermion ground state as predicted by the phase diagram in Fig. 2. At the lowest temperatures, an additional upturn of C/T with decreasing temperature is observed but no signs of ordering are apparent down to 0.37 K [Fig 4(b)], consistent with the electrical resistivity discussed in the next sections, which shows no signs of a phase transition down to 20 mK. A similar low-temperature upturn in C/T has previously been reported for off-stoichiometric CeCo_{0.89}Ge₂ [46]. Notably, the low-temperature anomaly exhibits little dependence on applied magnetic field (see Ref. [46]), suggesting that it may be an intrinsic feature rather than a Schottky anomaly arising from magnetic point defects or other extrinsic mechanisms. As seen in Fig. 4(c), the upturn approximately follows a logarithmic temperature dependence, $C/T \sim -\ln(T/T_0)$, a behavior often observed in the vicinity of quantum critical points, where $k_B T_0$ represents a characteristic energy scale associated with the quantum critical fluctuations [47]. In the present case, however, the magnitude of the increase is relatively small ($\approx 15 - 20$ %), which may indicate that CeCoGe₂ is located near, but not exactly at, the putative quantum crit-

ical point in the phase diagram. We obtain $T_0 = 2 - 5$ K (depending on the temperature range of the fit), consistent with this interpretation.

C. Electrical resistivity

Figure 5 shows the temperature-dependent electrical resistivity $\rho(T)$ of an as-grown CeCoGe₂ single crystal. Owing to the thin plate-like shape of the samples, measurements were only performed with current along the crystallographic *ac* plane. Different crystals from the same batch yield reproducible results with comparable values for the residual resistivities ($\rho_0 \approx 50 - 60 \mu\Omega \text{ cm}$) and residual resistivity ratios (RRR = 2.3 - 2.5). Both ρ_0 and RRR are also comparable to those reported for polycrystalline samples from Ref. [45], indicating that grain boundary scattering is not dominating the electrical transport. Indeed, as will be discussed later, the rather low RRR and sizeable ρ_0 is instead related to intrinsic Co vacancies, which lead to strong random potential fluctuations and impurity scattering of charge carriers. In contrast to CePtSi₂, there is almost no field dependence of $\rho(T)$ (less than 0.3% at 5 T), with a vanishingly small and positive transverse magnetoresistance [see inset of Fig. 5(a)].

We find that the low-temperature $\rho(T)$ behavior of CeCoGe₂ does not follow the conventional quadratic temperature dependence of Fermi liquids $\rho_{\text{FL}} = \rho_0 + AT^2$, but can instead be well described by a power law $\rho(T) = \rho_0 + AT^n$ with $n \approx 1.5$ [see Fig. 5(b)]. This behavior persists over an extended temperature range up to $T \approx 25$ K and appears to be correlated with the unit-cell volume (inset Fig. 5) as annealed crystals with contracted V display exponents closer to $n \approx 1.8$. It is known that disorder can modify the low-temperature exponent of $\rho(T)$, and anomalous non-Fermi-liquid (NFL) exponents, $n = 3/2$, have been associated with glassy behavior [48] and observed in various spin-glass and micromagnetic systems [6]. Another possibility is that the NFL exponent in CeCoGe₂ arises from its proximity to the putative quantum critical point indicated by the temperature–pressure phase diagram in Fig. 2 [49–53]. For comparison, CePtSi₂ has also revealed NFL behavior under pressure, close to the QCP and its superconducting dome. The inset of Figure 5(b) shows the exponent n of CePtSi₂ from Ref. [43] as a function of the unit-cell volume. At ambient pressure, $\rho(T)$ shows Fermi-liquid behavior with $n = 2$, but near the critical volume, the resistivity exponent drops to $n \approx 1$, and then increases to $n \approx 1.5 - 1.6$ at higher pressures (*i.e.* smaller volumes $V \approx 298 - 300 \text{ \AA}^3$). This may imply that CeCoGe₂ resides on the paramagnetic side of the quantum phase transition, in close proximity to, but not exactly at, the QCP. However, follow-up studies on higher-quality crystals and with continuous tuning parameters, such as magnetic field or uniaxial strain are required to determine whether CeCoGe₂ can be tuned to quantum criticality.

No signatures of superconductivity or magnetic order are observed down to 20 mK (Fig. 6).

D. Intrinsic defects

To elucidate the reason for the rather low RRR and high ρ_0 , we conducted single-crystal x-ray diffraction (XRD) experiments on several CeCoGe₂ single crystals. Our results show variation in the Co occupancy, consistent with previous reports on RECo_{*x*}Ge₂ germanides, which show a range of Co from 0.34 to 0.96 depending on the rare-earth (RE) element [33, 54]. Refinements of single-crystal XRD patterns reveal Co vacancies of the order of 4% ($x = 0.96$) in the crystals, which were grown from nominally stoichiometric CeCoGe₂ precursors dissolved in In flux, along with a slight deficiency of Ge on the Ge2 site ($\approx 98.7(4)\%$ occupancy). This prompted us to optimize the stoichiometry and try to suppress the Co vacancies by adding additional Co and Ge to the arc-melted precursor material used during the flux growth, resulting in nominal compositions of CeCo_{1+2*x*}Ge_{2+*x*}.

The observed phase of the resulting crystals and the concentration of Co vacancies as well as the residual resistivity ratios and resistivity exponents are summarized in Table 1. For $x > 0.2$, we find that CeCo₂Ge₂ crystals are formed, which belong to the tetragonal ThCr₂Si₂ structure type. Interestingly, against our expectations, for $x < 0.2$, the obtained CeCoGe₂ crystals display an even larger number of Co vacancies and even lower RRR values. We attribute this to a competition between the 112 (CeCoGe₂) and 122 (CeCo₂Ge₂) phases. Even for nominally stoichiometric CeCoGe₂, arc-melted samples displayed about 10–20% of the 122 phase, even after annealing for three weeks at 900 °C. We conclude that this behavior suggests either (i) the 112 phase is intrinsically unstable in its stoichiometric form and requires a small number of vacancies for stabilization, or (ii) a strong competition exists between the 112 and 122 phases, leading to off-stoichiometric variants of CeCoGe₂ as CeCo₂Ge₂ forms and depletes the molten solution of Co.

The fact that 4% Co vacancies result in a serious de-

TABLE I. Influence of starting stoichiometry on phase formation and transport quality of Ce-Co-Ge crystals grown by flux. Deviations from the nominal CeCoGe₂ composition do not improve crystal quality; instead, they increase Co deficiency and reduce the RRR, or stabilize the competing tetragonal CeCo₂Ge₂ phase. The exponent n is obtained from power law fits $\rho(T) = \rho_0 + AT^n$ to the low-temperature resistivity over an extended range of temperatures $T \lesssim 25$ K.

composition	observed phase	Co vacancies	RRR	n
CeCoGe ₂	CeCoGe ₂	4%	2.5	1.5–1.8
CeCo _{1.2} Ge _{2.1}	CeCoGe ₂	11%	1.5	1.3–1.6
CeCo _{1.4} Ge _{2.2} ,	CeCo ₂ Ge ₂	–	5.3	2
CeCo _{1.6} Ge _{2.3}				

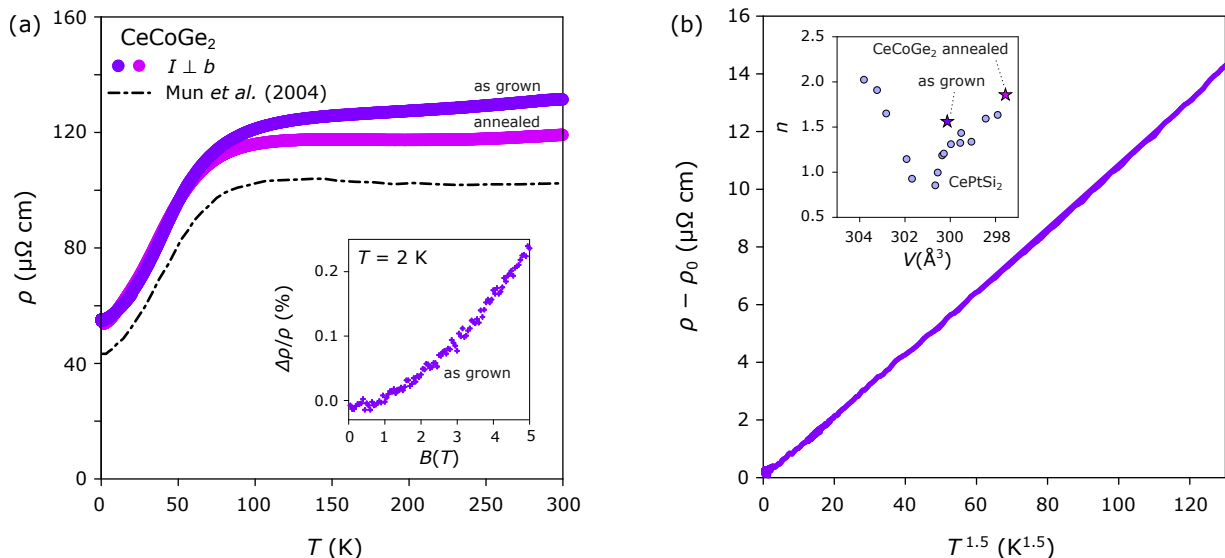


FIG. 5. Temperature-dependent electrical resistivity of CeCoGe_2 . (a) shows a comparison between our single crystals, where current was applied perpendicular to b , and the results for arc-melted polycrystalline CeCoGe_2 by Mun *et al.* [45] (black dashed-dotted line), which is about a factor of 1.4 smaller, while showing a comparable residual resistivity ratio $\text{RRR} \approx 2.5$. Inset shows negligible field dependence of the magnetoresistance at $T = 2$ K. (b) Low-temperature scaling of $\rho(T)$ follows a non-Fermi-liquid (NFL) behavior with $\rho(T) = \rho_0 + AT^n$ ($n \approx 1.5$). Inset shows unit-cell volume dependence of the resistivity exponent n for hydrostatic-pressure-tuned CePtSi_2 [43] and CeCoGe_2 at ambient pressure (this work).

terioration of the RRR and a sizeable residual resistivity, $\rho_0 \approx 50\text{--}60 \mu\Omega \text{ cm}$, suggests that Co $3d$ bands contribute significantly to the density of states near the Fermi level E_F (in agreement with density functional theory calculations [55]) and that Co site vacancies introduce strong disorder and decoherence for the Co $3d$ bands. Another possibility is that Co vacancies introduce nonhybridizing impurity states near E_F that can strongly scatter charge carriers from the bulk conduction bands, which is not uncommon for transition-metal site substitutions [56–63]. Figure 6 compares the temperature-dependent resistivity, normalized to its room-temperature value $\rho(T)/\rho(300 \text{ K})$, of CeCoGe_2 (this work) with single-crystal data for CePtSi_2 [37, 64], CeNiGe_2 [36] and CeRhGe_2 [37] from the literature. It is apparent that other CeTX_2 systems also suffer from rather low residual resistivity ratios, which can probably be related to intrinsic transition-metal vacancies as well. Indeed, intrinsic vacancies are ubiquitous in materials crystallizing in the CeNiSi_2 and the vacancy concentration depends sensitively on the rare-earth and transition metal element [33, 54]. In the case of CePtSi_2 , however, ρ_0 decreases significantly under applied magnetic field [64], indicating that the low RRR may be dominated by strong magnetic scattering and spin fluctuations near the antiferromagnetic transition, in contrast to the field-independent behavior observed in CeCoGe_2 (see inset Fig. 5a).

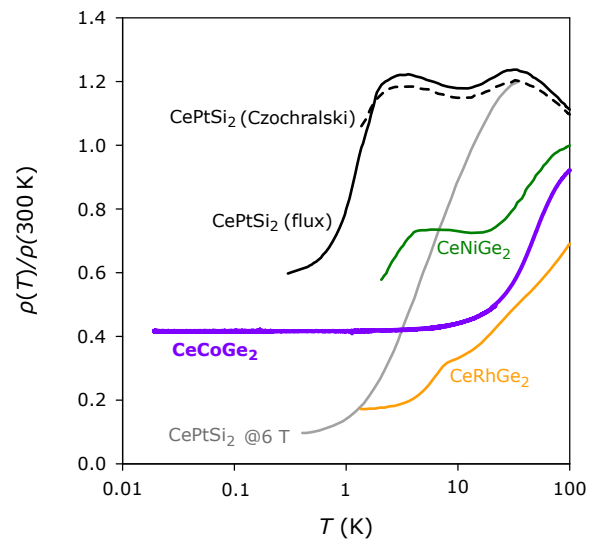


FIG. 6. Comparison of temperature-dependent resistivity normalized to room temperature $\rho(T)/\rho(300 \text{ K})$ for various single-crystalline CeTX_2 systems. Next to CeCoGe_2 , other CeTX_2 -based compounds also suffer from poor residual resistivity ratios. This suggests that intrinsic defects play an important role in the low-temperature transport properties of the CeNiSi_2 materials family in general.

IV. CONCLUSION

We compared the chemical and hydrostatic pressure dependence of locally noncentrosymmetric CeTX_2 -based materials, crystallizing in a pseudotetragonal, or-

thorhombic ($Cmcm$) structure, where T is a transition metal from the Fe, Co, Ni and Cu groups and X is either Si or Ge. The period of the transition metal and the unit-cell volume sensitively control the hybridization of the Ce $4f$ states with the conduction electrons, resulting in a putative QCP at a critical volume $V_c \approx 300 \text{ \AA}^3$, from which unconventional superconductivity emerges in CePtSi₂ and CeRhGe₂, both of which require hydrostatic pressure tuning. The large upper critical fields in CePtSi₂, about an order of magnitude above the Pauli limiting field, suggest a possible spin-triplet pairing. We identify CeCoGe₂ as a promising heavy-fermion compound sitting in proximity of the putative quantum critical point at ambient pressure. However, no superconductivity is detected down to 20 mK, which we attribute to the rather large residual resistivity. Single-crystal x-ray diffraction reveals intrinsic disorder in the form of Co-site vacancies, even in nominally stoichiometric samples that strongly affect electronic transport. Composition tuning further shows that these defects are likely intimately linked to a competing tetragonal phase (CeCo₂Ge₂) that forms at comparable temperatures.

V. ACKNOWLEDGEMENTS

Work at Los Alamos National Laboratory was performed under the auspices of the U.S. Department of Energy, Office of Basic Energy Sciences, Division of Materials Science and Engineering. F.G. acknowledges a Director's Postdoctoral Fellowship through the Laboratory and Directed Research & Development (LDRD) program. S.M.T. acknowledges support from the Los Alamos LDRD program. Scanning electron microscopy and energy-dispersive x-ray measurements were performed at the Center for Integrated Nanotechnologies, an Office of Science User Facility operated for the U.S. Department of Energy (DOE) Office of Science.

VI. APPENDIX

Figure 7 shows the field-dependent magnetization of an as-grown CeCoGe₂ single crystal. Magnetization data were obtained at 1.8 K with fields applied perpendicular and parallel to the crystallographic b -axis, showing linear behavior over the entire measured field range with no signs of saturation reaching values up to ≈ 0.09 and $0.036 \mu_B/\text{Ce}$ at 6.5 T for $H \perp b$ and $H \parallel b$, respectively.

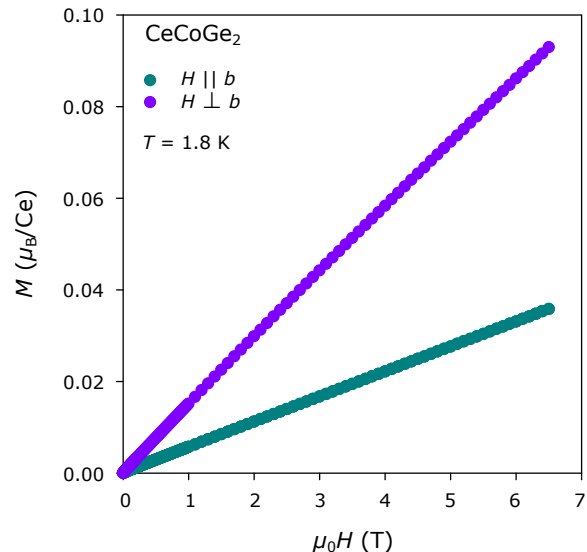


FIG. 7. Field-dependent magnetization of CeCoGe₂ single crystal as grown from In flux. Data were obtained at 1.8 K with fields applied perpendicular and parallel to the crystallographic b -axis, showing linear behavior over the entire measured field range.

-
- [1] S. G. Stewart, *Reviews of Modern Physics* **56**, 755 (1984).
- [2] Z. Fisk, D. Hess, C. Pethick, D. Pines, J. Smith, J. Thompson, and J. Willis, *Science* **239**, 33 (1988).
- [3] T. Park, F. Ronning, H. Yuan, M. Salamon, R. Movshovich, J. L. Sarrao, and J. D. Thompson, *Nature* **440**, 65 (2006).
- [4] P. Monthoux, D. Pines, and G. Lonzarich, *Nature* **450**, 1177 (2007).
- [5] Q. Si and F. Steglich, *Science* **329**, 1161 (2010).
- [6] J. A. Mydosh and P. M. Oppeneer, *Reviews of Modern Physics* **83**, 1301 (2011).
- [7] M. Sigrist and K. Ueda, *Reviews of Modern Physics* **63**, 239 (1991).
- [8] A. P. Mackenzie and Y. Maeno, *Reviews of Modern Physics* **75**, 657 (2003).
- [9] A. Huxley, I. Sheikin, E. Ressouche, N. Kernavanois, D. Braithwaite, R. Calemczuk, and J. Flouquet, *Physical Review B* **63**, 144519 (2001).
- [10] R. Joynt and L. Taillefer, *Reviews of Modern Physics* **74**, 235 (2002).
- [11] S. Ran, C. Eckberg, Q.-P. Ding, Y. Furukawa, T. Metz, S. R. Saha, I.-L. Liu, M. Zic, H. Kim, J. Paglione, *et al.*, *Science* **365**, 684 (2019).
- [12] C. Nayak, S. H. Simon, A. Stern, M. Freedman, and S. Das Sarma, *Reviews of Modern Physics* **80**, 1083 (2008).
- [13] S. D. Sarma, M. Freedman, and C. Nayak, *npj Quantum Information* **1**, 1 (2015).
- [14] K. Flensberg, F. von Oppen, and A. Stern, *Nature Reviews Materials* **6**, 944 (2021).
- [15] N. Read and D. Green, *Physical Review B* **61**, 10267 (2000).
- [16] G. E. Volovik, *The universe in a helium droplet*, Vol. 117 (OUP Oxford, 2003).
- [17] T. Rice and M. Sigrist, *Journal of Physics: Condensed Matter* **7**, L643 (1995).
- [18] P. Anderson, *Physical Review B* **32**, 499 (1985).
- [19] T. Hazra and P. Coleman, *Physical Review Letters* **130**, 136002 (2023).
- [20] C. Wälti, H. R. Ott, Z. Fisk, and J. L. Smith, *Physical Review Letters* **84**, 5616 (2000).
- [21] Y. Shimizu, D. Braithwaite, D. Aoki, B. Salce, and J.-P. Brison, *Physical Review Letters* **122**, 067001 (2019).
- [22] H. Tou, Y. Kitaoka, K. Ishida, K. Asayama, N. Kimura, E. Yamamoto, Y. Haga, K. Maezawa, *et al.*, *Physical Review Letters* **80**, 3129 (1998).
- [23] T. Hattori, Y. Ihara, Y. Nakai, K. Ishida, Y. Tada, S. Fujimoto, N. Kawakami, E. Osaki, K. Deguchi, N. Sato, *et al.*, *Physical Review Letters* **108**, 066403 (2012).
- [24] D. Aoki, K. Ishida, and J. Flouquet, *Journal of the Physical Society of Japan* **88**, 022001 (2019).
- [25] A. Mounce, H. Yasuoka, G. Koutroulakis, N. Ni, E. Bauer, F. Ronning, and J. Thompson, *Physical Review Letters* **114**, 127001 (2015).
- [26] D. Aoki, J.-P. Brison, J. Flouquet, K. Ishida, G. Knebel, Y. Tokunaga, and Y. Yanase, *Journal of Physics: Condensed Matter* **34**, 243002 (2022).
- [27] S. Khim, J. Landaeta, J. Banda, N. Bannor, M. Brando, P. Brydon, D. Hafner, R. KÜchler, R. Cardoso-Gil, U. Stockert, *et al.*, *Science* **373**, 1012 (2021).
- [28] S. Saxena, P. Agarwal, K. Ahilan, F. Grosche, R. Haselwimmer, M. Steiner, E. Pugh, I. Walker, S. Julian, P. Monthoux, *et al.*, *Nature* **406**, 587 (2000).
- [29] C. D. O'Neill, J. L. Schmehr, and A. D. Huxley, *Proceedings of the National Academy of Sciences* **119**, e2210235119 (2022).
- [30] Q. Li, Z.-N. Xiang, B.-B. Zhang, Y.-J. Zhang, C. Zhang, and H.-H. Wen, *arXiv preprint arXiv:2408.14334* (2024).
- [31] O. P. Squire, S. A. Hodgson, J. Chen, V. Fedoseev, C. K. de Podesta, T. I. Weinberger, P. L. Alireza, and F. M. Grosche, *Physical Review Letters* **131**, 026001 (2023).
- [32] T. Shi, W. Li, Q. Dong, P. Yang, H. Ma, Z. Tian, N. Wang, J. Sun, Y. Uwatoko, Y.-f. Yang, *et al.*, *arXiv preprint arXiv:2601.18476* (2026).
- [33] M. Francois, G. Venturini, B. Malaman, and B. Roques, *Journal of the Less Common Metals* **160**, 197 (1990).
- [34] W. Lee, K. Kwan, P. Klavins, and R. Shelton, *Physical Review B* **42**, 6542 (1990).
- [35] E. Cordruwisch, D. Kaczorowski, P. Rogl, A. Saccone, and R. Ferro, *Journal of Alloys and Compounds* **320**, 308 (2001).
- [36] M.-H. Jung, N. Harrison, A. H. Lacerda, H. Nakotte, P. Pagliuso, J. L. Sarrao, and J. D. Thompson, *Physical Review B* **66**, 054420 (2002).
- [37] Y. Hirose, N. Nishimura, F. Honda, K. Sugiyama, M. Hagiwara, K. Kindo, T. Takeuchi, E. Yamamoto, Y. Haga, M. Matsuura, *et al.*, *Journal of the Physical Society of Japan* **80**, 024711 (2011).
- [38] M. Szwalska, A. Gribanov, S. Gribanova, and D. Kaczorowski, *Journal of Alloys and Compounds* **735**, 855 (2018).
- [39] E. Mun, Y. Kwon, and M. Jung, *Physical Review B* **67**, 033103 (2003).
- [40] M. Pelizzone, H. Braun, and J. Muller, *Journal of Magnetism and Magnetic Materials* **30**, 33 (1982).
- [41] D. Adroja and B. Rainford, *Journal of Magnetism and Magnetic Materials* **119**, 54 (1993).
- [42] B. Chevalier, P. Rogl, K. Hiebl, and J. Etourneau, *Journal of Solid State Chemistry* **107**, 327 (1993).
- [43] T. Nakano, M. Ohashi, G. Oomi, K. Matsubayashi, and Y. Uwatoko, *Physical Review B—Condensed Matter and Materials Physics* **79**, 172507 (2009).
- [44] G. Oomi, T. Kagayama, Y. Uwatoko, H. Takahashi, and N. Mōri, *Journal of Alloys and Compounds* **207**, 278 (1994).
- [45] E. Mun, B. Lee, Y. Kwon, and M. Jung, *Physical Review B* **69**, 085113 (2004).
- [46] V. Pecharsky and K. Gschneidner Jr, *Physical Review B* **43**, 8238 (1991).
- [47] H. v. Löhneysen, A. Rosch, M. Vojta, and P. Wölfle, *Reviews of Modern Physics* **79**, 1015 (2007).
- [48] E. Miranda and V. Dobrosavljević, *Reports on Progress in Physics* **68**, 2337 (2005).
- [49] J. A. Hertz, in *Basic Notions of Condensed Matter Physics* (CRC Press, 2018) pp. 525–544.
- [50] A. Millis, *Physical Review B* **48**, 7183 (1993).
- [51] T. Moriya and T. Takimoto, *Journal of the Physical Society of Japan* **64**, 960 (1995).
- [52] S. Kambe, S. Raymond, L.-P. Regnault, J. Flouquet, P. Lejay, and P. Haen, *Journal of the Physical Society of Japan* **65**, 3294 (1996).

- [53] A. Rosch, *Physical Review Letters* **82**, 4280 (1999).
- [54] M. Méot-Meyer, G. Venturini, B. Malaman, and B. Roques, *Materials research bulletin* **20**, 1515 (1985).
- [55] H. C. Choi, K. Haule, G. Kotliar, B. Min, and J. Shim, *Physical Review B—Condensed Matter and Materials Physics* **88**, 125111 (2013).
- [56] M. Krishnan and V. Ganesan, *Journal of Physics: Condensed Matter* **32**, 335602 (2020).
- [57] F. Garmroudi, M. Parzer, A. Riss, A. V. Ruban, S. Khmelevskiy, M. Reticcioli, M. Knopf, H. Michor, A. Pustogow, T. Mori, *et al.*, *Nature Communications* **13**, 3599 (2022).
- [58] N. Reumann, A. Riss, F. Garmroudi, M. Parzer, J. Kovacevic, T. Mori, and E. Bauer, *Physical Review B* **106**, 235138 (2022).
- [59] F. Garmroudi, M. Parzer, A. Riss, A. Pustogow, T. Mori, and E. Bauer, *Physical Review B* **107**, L081108 (2023).
- [60] R. Jha, N. Tsujii, F. Garmroudi, S. Khmelevskiy, E. Bauer, and T. Mori, *Journal of Materials Chemistry C* **12**, 8861 (2024).
- [61] M. Parzer, F. Garmroudi, A. Riss, T. Mori, A. Pustogow, and E. Bauer, *Physical Review Letters* **135**, 066302 (2025).
- [62] M. Parzer, F. Garmroudi, A. Riss, M. Reticcioli, R. Podloucky, M. Stöger-Pollach, E. Constable, A. Pustogow, T. Mori, and E. Bauer, *PRX Energy* **3**, 033006 (2024).
- [63] G. Rogl, F. Garmroudi, A. Riss, X. Yan, J. Sereni, E. Bauer, and P. Rogl, *Intermetallics* **146**, 107567 (2022).
- [64] T. Nakano, S. Onuki, and N. Takeda, *Physica C: Superconductivity* **493**, 109 (2013).